JTTEE5 17:831–837
DOI: 10.1007/s11666-008-9239-4
1059-9630/$19.00 © ASM International

New Generation Perovskite Thermal Barrier Coating Materials

W. Ma, M.O. Jarligo, D.E. Mack, D. Pitzer, J. Malzbender, R. Vaßen, and D. Stöver

(Submitted June 13, 2008; in revised form August 6, 2008)

Advanced ceramic materials of perovskite structure have been developed for potential application in thermal barrier coating systems, in an effort to improve the properties of the pre-existing ones like yttria-stabilized zirconia. Yb_2O_3 and Gd_2O_3 doped strontium zirconate ($SrZrO_3$) and barium magnesium tantalate ($Ba(Mg_{1/3}Ta_{2/3})O_3$) of the ABO_3 and complex $A(B'_{1/3}B''_{2/3})O_3$ systems, respectively, have been synthesized using ball milling prior to solid state sintering. Thermal and mechanical investigations show desirable properties for high-temperature coating applications. On atmospheric plasma spraying, the newly developed thermal barrier coatings reveal promising thermal cycle lifetime up to 1350 °C.

Keywords gas turbine coatings, perovskite ceramics, plasma-sprayed TBCs, thermal cycling lifetime

1. Introduction

In the last two decades, much effort has been devoted to the development of ceramic thermal barrier coatings (TBCs) in order to increase the efficiency of gas turbines (Ref 1). State-of-the-art TBCs are usually based on 7-8 wt.% Y_2O_3-stabilized ZrO_2 (YSZ) prepared by atmospheric plasma spraying (APS) or electron-beam physical vapor deposition (EB-PVD) (Ref 2). The maximum surface temperature of these types of coatings is limited to ~1200 °C for long-term operations due to the phase transformation of zirconia. Such transformation results to change in volume and causes the formation of cracks in the coatings (Ref 3).

In order to remedy such phenomenon, a wide search has been conducted for new TBC materials which allow operation temperatures higher than 1200 °C without phase transformation, aside from thermochemical and thermomechanical compatibility with the substrate layer to be coated. Recently, perovskites (ABO_3) have been considered for this purpose. Such perovskites are usually characterized by melting point higher than 2000 °C. Further, the thermal expansion coefficient (TEC) has values typically greater than 8.5×10^{-6} K^{-1} and thermal conductivity of less than 2.2 W m^{-1} K^{-1}, which are advantageous for use as heat insulating layer (Ref 4). Perovskites additionally offer the possibility for extensive substitution of ions at *A* and/or *B* site, which enables the properties of the materials to be selectively influenced (Ref 5).

Among the perovskites, $SrZrO_3$ of ABO_3 and the complex $Ba(Mg_{1/3}Ta_{2/3})O_3$ of $A(B'_{1/3}B''_{2/3})O_3$ systems have been proven as two of the most refractory oxides known to science with melting temperature as high as 2650 °C (Ref 6) and 3100 °C (Ref 7, 8) respectively.

The $SrZrO_3$ perovskite undergoes three temperature-induced phase transformations, which are as follows (Ref 9):

$$\underset{Pnma}{\text{orthorhombic}} \xrightarrow{740^\circ C} \underset{Imma}{\text{pseudo-tetragonal}} \xrightarrow{840^\circ C} \underset{I4/mcm}{\text{tetragonal}} \xrightarrow{1130^\circ C} \underset{Pm\bar{3}m}{\text{cubic}},$$

a sequence entirely consistent with both Carlsson's observations (Ref 10). As a candidate TBC material, the phase transformations for $SrZrO_3$ are not desirable. However, there are no distinguishable discontinuities of the unit cell volumes in all of the structural phase transformations of $SrZrO_3$. Only the transformation from orthorhombic *Pnma* to pseudo-tetragonal *Imma* at 700 °C involves a small volume change of ~0.14% (Ref 11). These transformations are thus considered nearly continuous (Ref 12). On the other hand, formation of $Ba(Mg_{1/3}Ta_{2/3})O_3$ (BMT) is usually accompanied by secondary phases which as well are stable even after sintering at 1650 °C for a long time (Ref 13). Hence, such phenomena as phase transformation and occurrence of a secondary phase are not deemed obstacles in the synthesis and design of these potential perovskite ceramics for TBC applications.

This article is an invited paper selected from presentations at the 2008 International Thermal Spray Conference and has been expanded from the original presentation. It is simultaneously published in *Thermal Spray Crossing Borders, Proceedings of the 2008 International Thermal Spray Conference*, Maastricht, The Netherlands, June 2-4, 2008, Basil R. Marple, Margaret M. Hyland, Yuk-Chiu Lau, Chang-Jiu Li, Rogerio S. Lima, and Ghislain Montavon, Ed., ASM International, Materials Park, OH, 2008.

W. Ma, School of Materials Science and Engineering, Inner Mongolia University of Technology, Hohhot, P.R. China; and **M.O. Jarligo, D.E. Mack, D. Pitzer, J. Malzbender, R. Vaßen,** and **D. Stöver**, Institute of Energy Research, Forschungszentrum Jülich GmbH, Juelich, Germany. Contact e-mail: m.o.jarligo@fz-juelich.de.

The thermophysical properties of $SrZrO_3$ modified by doping with 10 mol% Yb_2O_3 and 20 mol% Gd_2O_3 and the complex BMT, together with their thermal cycling lifetime, are presented in this article.

2. Experimental Procedure

Solid-state synthesis of the modified $SrZrO_3$ was conducted through ball milling with ethanol the starting powders of Yb_2O_3 (Treibacher Powdermet, 99.9%), Gd_2O_3 (Treibacher Powdermet, 99.9%), $SrCO_3$ (Aldrich, >98%), and ZrO_2 (Aldrich, 99%). The milled suspension was then dried and calcined at 1400 °C. The synthesis procedure was repeated three times for the purpose of obtaining a single phase material. BMT, on the other hand, followed similar solid state route with starting powders of $BaCO_3$ (Alfa Aesar, 99.8%), MgO (Aldrich, >99%), and Ta_2O_5 (Treibacher Powdermet, 98.95%). After drying, the milled suspension was heat treated at 1500 °C for 48 h. The phases formed after syntheses were determined by XRD (Model D5000, Siemens, Cu K_α radiation, Germany).

Bulk specimens of $SrZrO_3$ and BMT materials were also prepared by cold pressing followed by sintering at 1600 °C for 6 h in air. The densities (ρ) of the sintered samples were measured according to Archimedes principle. Measurements of the thermal expansion coefficients (TECs), thermal diffusivities, and specific heat capacities of the bulk materials were then recorded by a high-temperature dilatometer (Model DIL 402E, Netzsch, Germany), laser flash (Model THETA, Netzsch, Germany), and simultaneous thermal analysis apparatus (Model STA 449C, Netzsch, Germany), respectively. The thermal conductivities of the sintered samples were calculated using the equation:

$$\lambda = D_{\text{th}}(T)C_p(T)\rho(T) \quad \text{(Eq 1)}$$

where λ, $D_{\text{th}}(T)$, $C_p(T)$, and $\rho(T)$ are the thermal conductivity, thermal diffusivity, specific heat capacity, and measured density, respectively.

For mechanical property measurements, the samples were prepared by cold-pressing and subsequent hot-pressing at 1550 °C with 100 MPa for 2-4 h. The prepared disc-shaped samples were cold mounted using resin and polished to ~1 μm. Young's modulus, hardness, and fracture toughness of the modified $SrZrO_3$ and BMT were determined by a depth-sensing microindentation technique in which the indenter position was precisely recorded at a given applied load. The instrument (Model H-100 Fischerscope, Helmut Fischer GmbH, Germany) displays the indenter displacement with accuracy in the nanometer range and a load resolution of 0.4 mN during the entire loading-unloading period.

For application as TBC topcoats, the synthesized $SrZrO_3$ and BMT powders were further milled with ethanol and 1.8 wt.% dispersing agent, then subsequently spray-dried. Sieved size fractions between 45 and 125 μm were used for plasma spraying. Single layer and double layer systems with 7.8 wt.% yttria-stabilized zirconia powder (Metco 204 NS, Sulzer Metco GmbH, Germany) underlayer were also prepared.

The modified $SrZrO_3$ coating, modified $SrZrO_3$/YSZ double layer coating (DLC), and BMT coating were air plasma sprayed (Triplex I gun, Sulzer Metco, Switzerland) on individual substrates such that a total coating thickness of about 400 μm was deposited. The conditions for the deposition of the coatings were argon and helium plasma gas flow rates of 20 and 13 standard liter per minute (slpm), a plasma current of 300 A at a power of 20 kW, and a spray distance of 100 mm. The DLC consisted of an YSZ coating directly sprayed on the bondcoat and a modified $SrZrO_3$ topcoat. Before deposition of the final topcoat, the substrates were coated with a 150 μm Ni-Co-Cr-Al-Y bondcoat by a vacuum plasma spray (VPS) in a Sulzer Metco facility using an F4 gun. The thickness of each topcoat was about half the total coating thickness.

For thermal cycling, the coatings were sprayed on IN738 substrate with diameter of 30 mm and thickness of 3 mm. The disc-shaped samples had beveled edges to minimize the effect of stresses originating from the free edges of the samples. During the manufacture of the thermal cycling specimens, steel substrates were also coated. These were used to characterize the as-sprayed condition of the coatings. The freestanding coatings, which were produced by removing the steel substrate from the sprayed coats with hydrochloric acid, were used to investigate the pore-size distribution using mercury porosimeters (Models Pascal 140 and 440, CE Instruments, Italy).

Thermal cycling was then carried out in a burner-rig test facility where samples were periodically heated and cooled. On heating, the reverse side of the samples was cooled by compressed air to maintain a temperature gradient of typically 0.4-1.0 K/μm across the samples. After the high-temperature phase, the burner was removed and the sample cooled with compressed air. The cycles usually took 5 min heating and 2 min cooling and were repeated until a clearly visible spallation of about 5×5 mm^2 of the coating occurred. The detailed process description can be found elsewhere (Ref 14).

The microstructure of the coatings was investigated by a scanning electron microscope (SEM) (Model JXA 840, JEOL, Japan).

3. Results and Discussion

3.1 Sintered Samples

The relative densities of the hot-pressed pellets are >95% of the theoretical densities. Moreover, the relative densities of the modified $SrZrO_3$ are slightly higher than that of pure $SrZrO_3$, indicating that doping Yb_2O_3 or Gd_2O_3 is favorable for the densification of $SrZrO_3$. These samples were further used for determination of mechanical properties.

The TECs of the dense $SrZrO_3$, $Sr(Zr_{0.9}Yb_{0.1})O_{2.95}$, $Sr(Zr_{0.8}Gd_{0.2})O_{2.9}$, and BMT are shown subsequently (Fig. 1). The TEC of $SrZrO_3$ is 8.7-10.8 $\times 10^{-6}$ K^{-1}

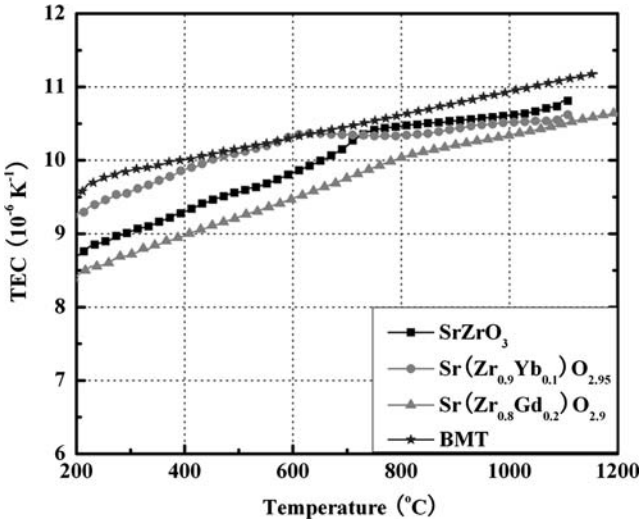

Fig. 1 TEC profiles for $SrZrO_3$, $Sr(Zr_{0.9}Yb_{0.1})O_{2.95}$, $Sr(Zr_{0.8}Gd_{0.2})O_{2.9}$, and BMT bulk materials

(200-1100 °C), which is comparable to that of YSZ (~10.5 × 10^{-6} K^{-1}, 200-1100 °C) (Ref 15). The slope of the TEC profile for $SrZrO_3$ slightly changed at ~750 °C, which is in accordance with a phase transformation from orthorhombic to pseudo-tetragonal. The TEC of $Sr(Zr_{0.9}Yb_{0.1})O_{2.95}$ is higher below ~740 °C and comparable between 740 and 1100 °C to that of $SrZrO_3$. The change in the slope of the TEC profile at ~630 °C is much lower than that of $SrZrO_3$, indicating that doping Yb_2O_3 can shift the phase transformation temperature to a lower temperature range. As for $Sr(Zr_{0.8}Gd_{0.2})O_{2.9}$, TEC is lower than that of $SrZrO_3$ all throughout the measured temperature range. A lower TEC may lead to higher stress generation during thermal cycling, which is a disadvantage for TBC application. However, the TEC of $Sr(Zr_{0.8}Gd_{0.2})O_{2.9}$ has no obvious abnormal change during measurement, indicating that doping with Gd_2O_3 can enhance the phase stability of $SrZrO_3$. This might be due to a larger octahedral factor of r_{Gd}/r_O compared with r_{Yb}/r_O in perovskite structure, r_i being the ionic radius.

BMT, on the other hand, gave the highest and consistent TEC profile from 200 to 1100 °C, indicating no structural transformation despite the presence of minor secondary phases of $BaTa_2O_6$ and $Ba_4Ta_2O_9$ in the test sample. The higher TEC for BMT is beneficial for TBC application, because it can alleviate stress misfit between topcoat and bondcoat, as well as substrate super alloy during thermal cycling. However, at the moment, the data for thermal cycling of BMT are still being generated and will be reported later.

Specific heat capacity (C_p) profiles reveal that BMT has the lowest C_p, followed by $Sr(Zr_{0.8}Gd_{0.2})O_{2.9}$, $Sr(Zr_{0.9}Yb_{0.1})O_{2.95}$, and $SrZrO_3$ consecutively (Fig. 2). Doping with Yb_2O_3 and Gd_2O_3 does not only suppress the phase transformations in $SrZrO_3$, but also lower its C_p value. This doping effect also yields a lower thermal conductivity for a given thermal diffusivity value at the temperature range of 200-1200 °C.

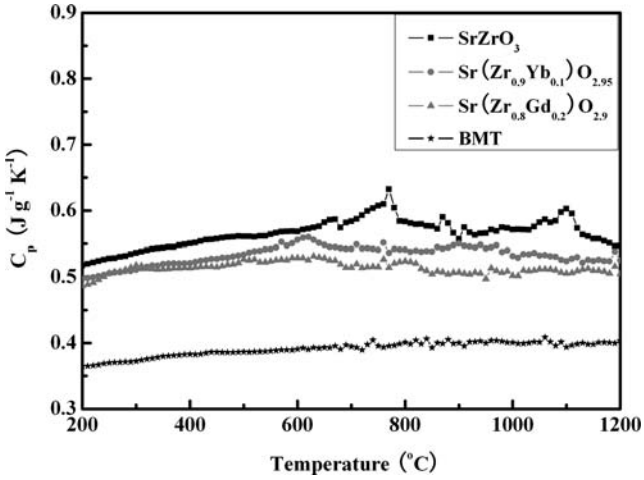

Fig. 2 Specific heat capacity profiles for $SrZrO_3$, $Sr(Zr_{0.9}Yb_{0.1})O_{2.95}$, $Sr(Zr_{0.8}Gd_{0.2})O_{2.9}$, and BMT

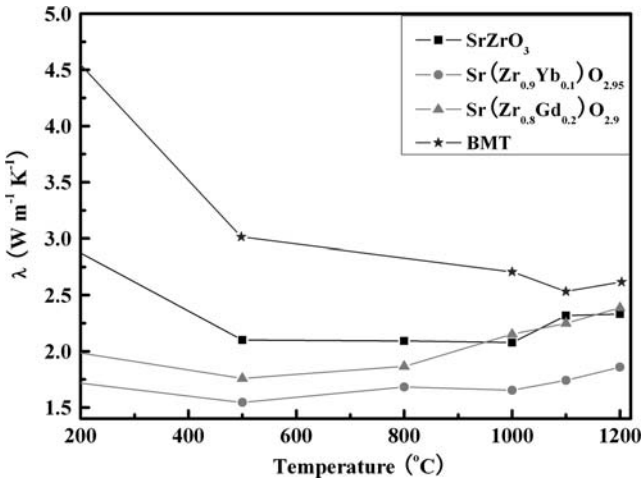

Fig. 3 Thermal conductivities of $SrZrO_3$, $Sr(Zr_{0.9}Yb_{0.1})O_{2.95}$, $Sr(Zr_{0.8}Gd_{0.2})O_{2.9}$, and BMT as a function of temperature

The thermal conductivity of these materials decreases with increase in temperature up to about 500 °C where the profiles suggest a rather constant value up to 1000 °C. After which, the thermal conductivity profiles continue to increase with further temperature rise, except for BMT which further decreases in value (Fig. 3). The thermal conductivity for $Sr(Zr_{0.9}Yb_{0.1})O_{2.95}$ reveals a very promising profile in that it is not only at least ~20% lower than that of $SrZrO_3$, but also ~20% lower than that of YSZ at 1000 °C (2.1-2.2 W m^{-1} K^{-1}, 1000 °C) (Ref 16). The thermal conductivity of $(Zr_{0.8}Gd_{0.2})O_{2.9}$ is lower below ~900 °C and comparable between 900 and 1100 °C to that of $SrZrO_3$. These results reveal that doping with Yb_2O_3 is more efficient in reducing the thermal conductivity of $SrZrO_3$ than doping with Gd_2O_3. BMT has the highest thermal conductivity among the four materials, which could be attributed to its higher thermal diffusivity and bulk density compared to the other three materials.

Table 1 Mechanical properties of bulk materials

Material	Young's modulus, GPa	Hardness, GPa	Fracture toughness, MPa·m$^{1/2}$
$SrZrO_3$	170 ± 4	13 ± 1	1.5 ± 0.1
$Sr(Zr_{0.8}Gd_{0.2})O_{2.9}$	160 ± 5	9.2 ± 0.3	1-2
$Sr(Zr_{0.9}Yb_{0.1})O_{2.95}$	150 ± 5	9.2 ± 0.9	1-2
BMT	186 ± 2	12 ± 2	~0.7
YSZ (Ref 17)	210 ± 10	13 ± 1	~3

It is uncertain if the increasing values of the thermal conductivity at high temperatures above 1000 °C in Fig. 3 are realistic. This increase could probably be due to the method of thermal diffusivity measurement, which is the laser flash technique. Such technique requires a supplementary topcoat to make the test sample opaque at measurements above 1000 °C, because ceramic materials are transparent on thermal radiation to a certain extent in this temperature region. The opaque layer, which was graphite in this case, tends to disintegrate at elevated temperatures. This can lead to erroneous values of the thermal diffusivity, and usually the value at high temperatures could therefore be too high.

The mechanical properties of $SrZrO_3$ and BMT were determined by an indentation technique (Table 1). Values for YSZ are also listed for reference. The Young's modulus of the modified $SrZrO_3$ was found to be lower than that of $SrZrO_3$. A low elastic modulus value is advantageous with respect to thermal stresses. The fracture toughness of the modified $SrZrO_3$ is between 1.0 and 2.0 MPa·m$^{1/2}$, which is comparable to that of YSZ (1-2 MPa·m$^{1/2}$) (Ref 17) and $SrZrO_3$ (1.5 ± 0.1 MPa·m$^{1/2}$). BMT, on the other hand, has the lowest value of fracture toughness, which might be associated with an inhomogeneity of the material due to the secondary phases present.

3.2 Plasma-Sprayed Coatings

Plasma-sprayed coatings of $Sr(Zr_{0.9}Yb_{0.1})O_{2.95}$, $Sr(Zr_{0.8}Gd_{0.2})O_{2.9}$, and BMT were first optimized mainly with respect to homogeneity of the microstructure. The porosity distribution of modified $SrZrO_3$ and BMT coatings used for thermal cycling is shown in Fig. 4. The porosity distribution of $SrZrO_3$ coating is also presented for comparison. The results reveal a typical bimodal pore size distribution. The larger defects corresponding to radii above 1 μm are believed to have resulted from macrocracks and voids. The fine pores smaller than 1 μm are mainly attributed to microcracks such as intersplat gaps and intrasplat cracks. The cumulative porosities of the freestanding coatings are ~20.0, ~16.5, and ~15.0% for $Sr(Zr_{0.9}Yb_{0.1})O_{2.95}$, $Sr(Zr_{0.8}Gd_{0.2})O_{2.9}$, and BMT, respectively. The modified $SrZrO_3$ coatings have slightly larger values than the optimized porosity level (~15%) normally used in conventional YSZ-based TBCs (Ref 18). $SrZrO_3$ coating has a lower cumulative porosity than the other three coatings with almost no macrocracks and voids. This could be attributed to the smaller particle size used for plasma spraying (56-90 μm). The smaller particles of

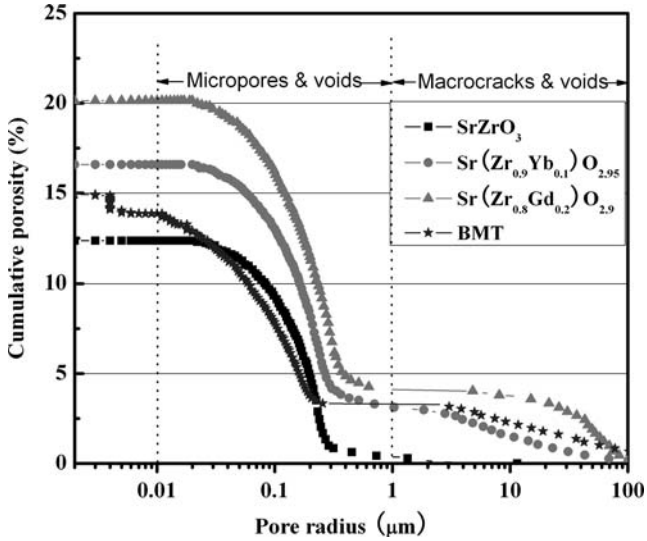

Fig. 4 Porosity distribution of $Sr(Zr_{0.9}Yb_{0.1})O_{2.95}$, $Sr(Zr_{0.8}Gd_{0.2})O_{2.9}$, and BMT freestanding coatings in the as-sprayed state

Table 2 Thermal cycling test results

TBC system	$T_{surf.}$, °C	$T_{sub.}$, °C	Cycles to failure
$SrZrO_3$	1251	965	1514
$Sr(Zr_{0.8}Gd_{0.2})O_{2.9}$	1130	984	13
$Sr(Zr_{0.8}Gd_{0.2})O_{2.9}$/YSZ	1249	965	3853
	1348	1015	208
$Sr(Zr_{0.9}Yb_{0.1})O_{2.95}$/YSZ	1246	974	3443
	1329	1011	1285
$Sr(Zr_{0.9}Yb_{0.1})O_{2.95}$	1239	969	806
$Ba(Mg_{0.33}Ta_{0.67})O_3$/YSZ	1242	1038	560
Typical YSZ (Ref 20)	1320-1350	1000-1035	250-1000

$T_{surf.}$ is the surface temperature, while $T_{sub.}$ is the substrate temperature of a sample

$SrZrO_3$ must have been well melted and ultimately formed a denser coating.

The thermal cycling results for $Sr(Zr_{0.9}Yb_{0.1})O_{2.95}$/YSZ and $Sr(Zr_{0.8}Gd_{0.2})O_{2.9}$/YSZ DLC are listed in Table 2. Typical values for YSZ coatings are also presented for comparison. It is obvious that the single layer $Sr(Zr_{0.9}Yb_{0.1})O_{2.95}$ and $Sr(Zr_{0.8}Gd_{0.2})O_{2.9}$ coatings have shorter thermal cycling lifetime compared to that of the lone YSZ coating. However, the thermal cycling lifetimes of the DLCs $Sr(Zr_{0.9}Yb_{0.1})O_{2.95}$/YSZ and $Sr(Zr_{0.8}Gd_{0.2})O_{2.9}$/YSZ at a surface temperature of ~1250 °C are 3443 cycles and 3853 cycles, respectively, which are comparable to that of YSZ and much higher than that of $SrZrO_3$. This indicates that the DLC system can indeed prolong the thermal cycling lifetime of new TBC materials.

At a surface temperature >1300 °C, the thermal cycling lifetime of $Sr(Zr_{0.9}Yb_{0.1})O_{2.95}$/YSZ coating is 1285 cycles, which appears rather long, whereas the lifetime of $Sr(Zr_{0.8}Gd_{0.2})O_{2.9}$/YSZ coating is much shorter. The shorter coating lifetime of the newly developed materials

might be mainly due to the lower critical energy release rate as compared to that of YSZ. Lower critical energy release rate has a higher potential for bondcoat-ceramic delamination (Ref 19).

The surface morphology of the $Sr(Zr_{0.9}Yb_{0.1})O_{2.95}$/YSZ coating after cycling at a surface temperature of 1329 °C reveals some spalling of the topcoat from the bondcoat (Fig. 5a). Its corresponding cross-section micrograph also reveals some vertical cracks that might have developed due to the sintering of the coating surface, which is also observed in YSZ coating after cycling at surface temperature range between 1320 and 1350 °C (Ref 20).

The surface morphology of $Sr(Zr_{0.8}Gd_{0.2})O_{2.9}$/YSZ coating after thermal cycling at a surface temperature of 1348 °C reveals that sintering of the coating surface occurred (Fig. 5b). The corresponding cross-section micrograph shows the formation of parallel cracks at the YSZ-$Sr(Zr_{0.8}Gd_{0.2})O_{2.9}$ interface and vertical cracks in the $Sr(Zr_{0.8}Gd_{0.2})O_{2.9}$ layer. The development of parallel cracks is mainly attributed to the lower TEC of $Sr(Zr_{0.8}Gd_{0.2})O_{2.9}$ as compared to YSZ. The surface coating spalled from the $Sr(Zr_{0.8}Gd_{0.2})O_{2.9}$ layer as confirmed by the XRD profile in Fig. 6(A), which reveals that YSZ diffraction peak after thermal cycling is absent.

The surface XRD patterns of $Sr(Zr_{0.9}Yb_{0.1})O_{2.95}$/YSZ and $Sr(Zr_{0.8}Gd_{0.2})O_{2.9}$/YSZ DLC as-sprayed and after cycling at different surface temperatures are shown in Fig. 6(a). The DLC is single phase in the as-sprayed condition. However, after thermal cycling at high surface temperatures (~1250 or ~1350 °C), secondary phases appeared, which are Yb_2O_3 for $Sr(Zr_{0.9}Yb_{0.1})O_{2.95}$/YSZ and Gd_2O_3 for the $Sr(Zr_{0.8}Gd_{0.2})O_{2.9}$/YSZ. The precipitation of the secondary phase in the coatings is detrimental for TBC applications.

During thermal cycling, different vapor pressures for ZrO_2, SrO, Yb_2O_3, and Gd_2O_3, which are 1×10^{-6} atm (2500 °C), 2×10^{-5} atm (2500 °C), 6×10^{-8} atm (2500 °C), and 9×10^{-6} atm (2500 °C), respectively, are believed to be the cause of the precipitation phenomenon (Ref 21, 22). According to the ZrO_2-SrO phase diagram (Ref 6), during thermal spraying, SrO volatilizes more than ZrO_2 due to its higher vapor pressure, resulting in the deviation of the coating composition from stoichiometric $SrZrO_3$. Zr is partially substituted in $SrZrO_3$ by Yb or Gd, and the vapor pressure of SrO is higher than that of both Yb_2O_3 and Gd_2O_3. Therefore the mixture of $SrZrO_3$ and the small amount of non-equilibrium Yb_2O_3 or Gd_2O_3 is believed to be present in the as-sprayed coatings. The non-equilibrium Yb_2O_3 or Gd_2O_3 transforms into equilibrium phase upon cycling, as well as the amount of Yb_2O_3 or Gd_2O_3 in the coatings increases simultaneously, which might be due to their limited

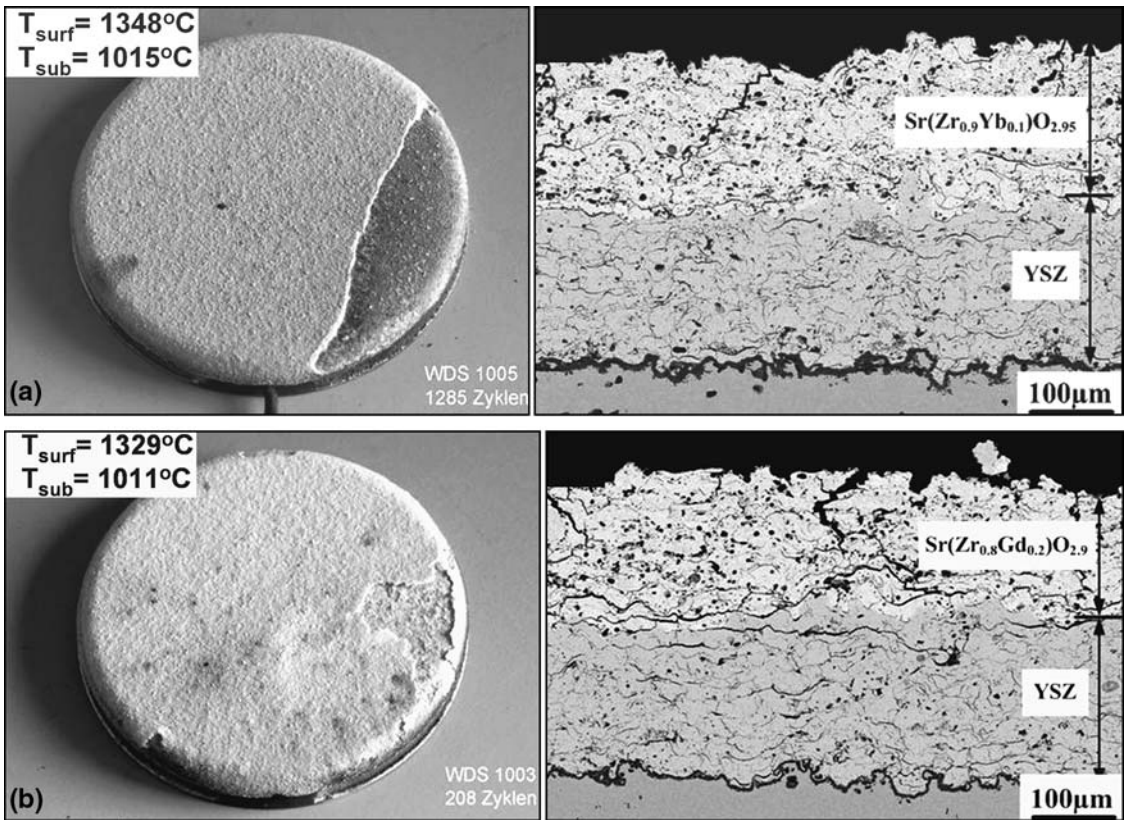

Fig. 5 Surface morphology and corresponding cross-section micrographs after thermal cycling of the double layer coatings of (a) $Sr(Zr_{0.9}Yb_{0.1})O_{2.95}$/YSZ and (b) $Sr(Zr_{0.8}Gd_{0.2})O_{2.9}$/YSZ

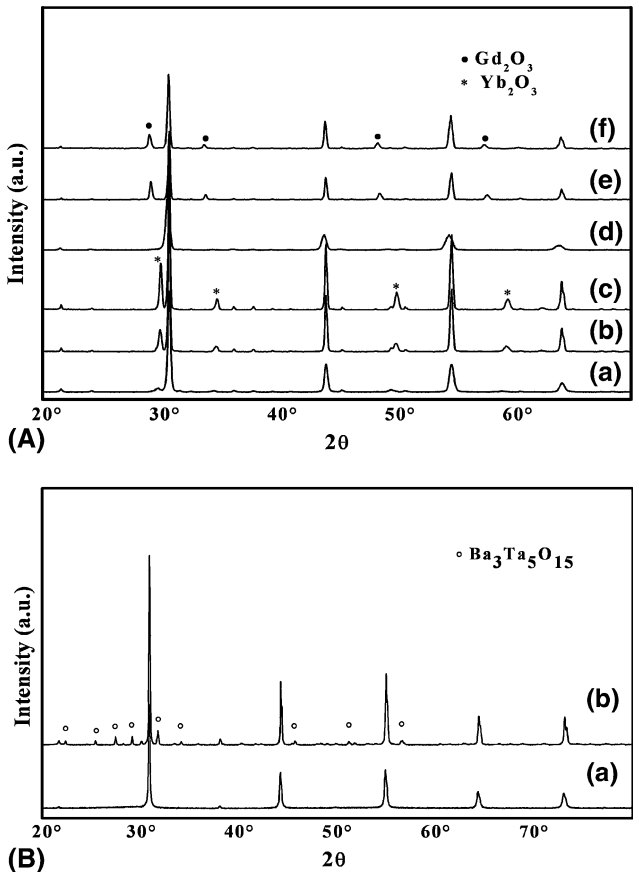

Fig. 6 (A) XRD profiles of the surface of $Sr(Zr_{0.9}Yb_{0.1})O_{2.95}$/YSZ coating in (a) as-sprayed, after cycling at surface temperature of (b) 1246 °C and (c) 1329 °C, and for $Sr(Zr_{0.8}Gd_{0.2})O_{2.9}$/YSZ coating (d) as-sprayed, after cycling at surface temperature of (e) 1249 °C and (f) 1348 °C. (B) XRD profiles of the surface of BMT/YSZ coating in the (a) as-sprayed and (b) after cycling at surface temperature of 1242 °C

solubility in $SrZrO_3$ at lower temperatures as compared to the synthesis temperature of $Sr(Zr_{0.9}Yb_{0.1})O_{2.95}$ and $Sr(Zr_{0.8}Gd_{0.2})O_{2.9}$. The lifetime values of the designed TBCs, however, suggest that the double layer systems of the modified $SrZrO_3$ paired with YSZ could be alternatives for high-temperature applications than possible with lone YSZ coating.

For the double layer BMT/YSZ system, the thermal cycling lifetime is lower compared to the other DLC systems of the modified $SrZrO_3$ owing to its much lower fracture toughness, higher elastic modulus, and higher thermal diffusivity. Such factors greatly influence the material response to stresses resulting from thermal mismatch between the different layer materials (Ref 23). Moreover, some thermal instabilities were observed during the thermal cycling test of the BMT TBC, which could be due to the formation of $Ba_3Ta_5O_{15}$ as revealed in the XRD profile of the cycled sample in Fig. 6(B). The thermal cycling lifetime of 560 cycles at ~1250 °C is nevertheless promising at this early stage of investigation for BMT as a thermal barrier coating material.

4. Conclusions

Perovskite $Sr(Zr_{0.9}Yb_{0.1})O_{2.95}$, $Sr(Zr_{0.8}Gd_{0.2})O_{2.9}$, and BMT were investigated for their potential as new generation TBC materials. The TECs of $Sr(Zr_{0.9}Yb_{0.1})O_{2.95}$ and BMT are 9.2-10.6 $\times 10^{-6}$ K^{-1} (200-1100 °C) and 9.5-11.1 $\times 10^{-6}$ K^{-1} (200-1100 °C), respectively, which are comparable to that of YSZ, while $Sr(Zr_{0.8}Gd_{0.2})O_{2.9}$ on the other hand has a lower TEC value. The results of specific heat capacity and thermal conductivity measurements reveal that doping Yb_2O_3 is more effective in reducing the specific heat capacity and thermal conductivity of $SrZrO_3$ than doping Gd_2O_3. The thermal conductivity of $Sr(Zr_{0.9}Yb_{0.1})O_{2.95}$ is ~20% lower than that of $SrZrO_3$ within the temperature range of 200-1200 °C, which is beneficial for thermal insulation. Whereas BMT has the highest thermal conductivity among the four materials which could be attributed to its higher thermal diffusivity and bulk density, even with the lowest specific heat capacity. Nevertheless, the potential for its applicability in TBC systems is very promising due to (comparable or better) properties than YSZ.

The Young's moduli of the modified $SrZrO_3$ were found to be lower than that of YSZ, which might yield higher strain tolerance for coatings. Furthermore, compared to thermal cycling lifetime of the single layer $Sr(Zr_{0.9}Yb_{0.1})O_{2.95}$ and $Sr(Zr_{0.8}Gd_{0.2})O_{2.9}$ coatings, $Sr(Zr_{0.9}Yb_{0.1})O_{2.95}$/YSZ and $Sr(Zr_{0.8}Gd_{0.2})O_{2.9}$/YSZ DLCs have much longer thermal cycling lifetimes at a surface temperature of ~1250 °C, which are comparable to that of the YSZ coating at similar surface temperature. A major advantage of the $Sr(Zr_{0.9}Yb_{0.1})O_{2.95}$/YSZ DLC is that its thermal cycling lifetime is better compared to that of the optimized single layer YSZ topcoat at a surface temperature of ~1350 °C. This suggests that double layer coatings with Yb-modified $SrZrO_3$ could be alternatives for lone YSZ coating at higher temperature applications.

Compared to the $SrZrO_3$ coatings, low fracture toughness, higher elastic modulus, and decomposition of BMT lead to its earlier failure at ~1250 °C.

Acknowledgments

The authors would like to thank the staff of Forschungszentrum Juelich most especially those from IEF-1, IEF-2, and B-NM who in one way or another contributed to the fulfillment of this study.

References

1. R.A. Miller, Thermal Barrier Coatings for Aircraft Engines: History and Directions, *J. Therm. Spray Technol.*, 1997, **6**(13), p 35-42
2. W.A. Nelson and R.M. Orenstein, TBC Experience in Land/Based Gas Turbines, *J. Therm. Spray Technol.*, 1997, **6**(2), p 176-180
3. R.A. Miller, J.L. Smialek, and R.G. Garlick, Phase Stability in Plasma-Sprayed Partially Stabilized Zirconia-Yttria. Advances in Ceramics, Vol. 3, Science and Technology of Zirconia, A.H. Heuer and L.W. Hobbs, Eds., Columbus, OH: American Ceramic Society, 1981, p 241-251

4. R. Vassen, S. Schwartz-Luckge, W. Jungen, and D. Stoever, Heat-Insulating Layer Made of Complex Perovskite, US Patent 20050260435 A1, 2005
5. B. Heimberg, W. Beele, K. Kempter, U. Bast, T. Haubold, M. Hoffmann, A. Endriss, P. Greil, C. Hong, F. Aldinger, and H. Seifert, Process for Production a Ceramic Thermal Barrier Layer for Gas Turbine Engine Component, US Patent 6602553 B2, 2003
6. T. Noguchi, T. Okubo, and O. Yonemochi, Reactions in the System ZrO_2-SrO, *J. Am. Ceram. Soc.*, 1969, **52**(4), p 178-181
7. R. Guo, A.S. Bhalla, and L.E. Cross, $Ba(Mg_{1/3}Ta_{2/3})O_3$ Single Crystal Fiber Grown by the Laser Heated Pedestal Growth Technique, *J. Appl. Phys.*, 1994, **75**(9), p 4704-4708
8. A.S. Bhalla and R. Guo, Design of Dielectric Substrates for High TC Superconductor Films, *Acta Phys. Pol. A*, 1997, **92**, p 7-21
9. C.J. Howard, K.S. Knight, B.J. Kennedy, and E.H. Kisi, The Structural Phase Transitions in Strontium Zirconate Revisited, *J. Phys.: Condens. Matter.*, 2000, **12**, p L677-L683
10. L. Carlsson, High-Temperature Phase Transitions in $SrZrO_3$, *Acta Crystallogr.*, 1967, **23**, p 901-905
11. D. Ligny and P. Richet, High-Temperature Heat Capacity and Thermal Expansion of $SrTiO_3$ and $SrZrO_3$ Perovskites, *Phys. Rev. B*, 1996, **53**(6), p 3013-3022
12. Y. Zhao and D.J. Weidner, Thermal Expansion of $SrZrO_3$ and $BaZrO_3$ Perovskites, *Phys. Chem. Miner.*, 1991, **18**, p 294-301
13. Y. Fang, A. Hu, S. Ouyang, and J. Jei Oh, The Effect of Calcination on the Microwave Dielectric Properties of $Ba(Mg_{1/3}Ta_{2/3})O_3$, *J. Eur. Ceram. Soc.*, 2001, **21**, p 2745-2750
14. F. Traeger, R. Vassen, K.-H. Rauwald, and D. Stöver, Thermal Cycling Setup for Testing Thermal Barrier Coatings, *Adv. Eng. Mater.*, 2003, **5**(6), p 429-433
15. R. Morrell, Handbook of Properties of Technical and Engineering Ceramics, Part 1. Her Majesty's Stationery Office, London, 1989
16. R. Vassen, F. Tietz, G. Kerkhoff, R. Wilkenhoener, and D. Stoever, New Materials for Advanced Thermal Barrier Coatings, *Proceedings of the 6th Liège Conference, Part III, Materials for Advanced Power Engineering*, J. Lecomte-Beckers, F. Schubert, and P.J. Ennis, Eds., Forschungszentrum Jülich GmbH, Jülich, Germany, 1998, p 162-165
17. C. Mercer, J.R. Williams, D.R. Clarke, and A.G. Evans, On a Ferroelastic Mechanism Governing the Toughness of Metastable Tetragonal Prime (t′) Yttria-Stabilized Zirconia, *Proc. R. Soc. A*, 2007, **463**, p 1393-1408
18. S. Stecura, Optimization of the Ni-Cr-Al-Y/ZrO_2-Y_2O_3 Thermal Barrier System, *Adv. Ceram. Mater.*, 1986, **1**(1), p 68-76
19. U. Bast and E. Schumann, Development of Novel Oxide Materials for TBCs, *Ceram. Eng. Sci. Proc.*, 2002, **23**, p 525-532
20. F. Traeger, M. Ahrens, R. Vassen, and D. Stoever, A Life Time Model for Ceramic Thermal Barrier Coatings, *Mater. Sci. Eng. A*, 2003, **358**, p 255-265
21. N. Jacobson, Thermodynamic Properties of Some Metal Oxide-Zirconia Systems, NASA TM 102351, 1989
22. U. Schulz, B. Saruhan, K. Fritscher, and C. Leyens, Review on Advanced EB-PVD Ceramic Topcoats for TBC Applications, *Int. J. Appl. Ceram. Technol.*, 2004, **1**(4), p 302-315
23. D. Schwingel, R. Taylor, T. Haubold, J. Wigren, and C. Gualco, Mechanical and Thermophysical Properties of Thick PYSZ Thermal Barrier Coatings: Correlation with Microstructure and Spraying Parameters, *Surf. Coat. Technol.*, 1998, **108-109**(1-3), p 99-106